PERGAMON

International Journal of Solids and Structures 37 (2000) 6063–6083

INTERNATIONAL JOURNAL OF SOLIDS and STRUCTURES

www.elsevier.com/locate/ijsolstr

Simulation of closed thin-walled structures partially filled with fluid

R. van Dijk*, F. van Keulen, J.C. Sterk

Faculty of Design, Engineering and Production, TU Delft, P.O. Box 5033, 2600 GA, Delft, The Netherlands

Received 26 February 1999; in revised form 1 October 1999

Abstract

For closed structures, the enclosed gas volume can contribute significantly to the strength and stiffness of a structure. The present paper describes the use of a gas element which is incorporated into finite elements for shells. In addition, a method to solve the governing set of equations efficiently is described. The method has been applied to a typical packaging example, namely a closed filled bottle. To validate the proposed method, numerical studies have been compared with experiments. © 2000 Elsevier Science Ltd. All rights reserved.

Keywords: Gas; Pressure; Shells; Finite element; Compression; Pneumatic element; Fluid; Bottles

1. Introduction

Many thin-walled structures surround a volume. Typical examples are filled bags, bottles, soft drink cans, tires, balloons, athletic shoes with air compartments, etc. Deformation of such structures causes internal pressure changes and may therefore influence the mechanical properties significantly. For example, a buckling load can increase.

The present research originated from the fact that it was desirable for Unilever, a large manufacturer of food products, to determine the compression strength of closed filled bottles for edible oil. Effective tools for simulation of the filled packages makes it possible to achieve more competitive designs at acceptable design or reduced design costs.

In many Finite Element (FE) programs it is not possible to include this pressure effect easily. However, the FEA program ABAQUS (ABAQUS, 1995) contains elements for solving problems involving fluid-filled cavities under hydrostatic conditions. Among others (Bucklin et al., 1985; Esslinger

* Corresponding author. Fax: +31-15-278-2150.
E-mail address: r.vandijk@wbmt.tudelft.nl (R. van Dijk).

0020-7683/00/$ - see front matter
PII: S0020-7683(99)00287-5

and Geier, 1976; Harris, 1957; Fung and Sechler, 1957; Goree and Nash, 1962; Weingarten et al., 1965; Seide, 1962), Berry (1996) investigated internal pressure effects. The modelling was done using a pneumatic element which relates the pressure to the internal enclosed volume. Applications that were considered are pressurized soft drink cans and an air spring. The formulation of the pneumatic element is started from the virtual work principle. The virtual work equation is augmented to account for the virtual work corresponding to the pressure of the enclosed gas. The latter can easily be determined using the corresponding gas law. The solution of the governing set of equations has not been addressed by Berry (1996). Due to the fact that the pressure causes the system matrix to be non-sparse, solving the set of equations, using a direct solver, is not obvious and will be described in the present paper. The results of the described method have been compared with experimental and numerical results reported by Berry (1996).

Other complications that were encountered involved a reversing of the pressure. If during an incremental-iterative solution procedure the incremental volume change of the structure is larger than the remaining gas volume, then the new gas volume becomes negative, consequently leading to a negative pressure. Obviously, this situation is physically infeasible. This effect manifests itself mainly for relatively small enclosed gas volumes. This situation is typical for many packages. By introducing a fluid compliance, this numerical complication has been circumvented.

The present work can be divided in different parts. Firstly, a theoretical description is given which describes how the contents, gas and fluid, influence on the internal gas pressure. Furthermore, this section describes the prevention of the pressure reverse discussed earlier. Secondly, implementational issues and solution of the non-sparse stiffness matrix are addressed. Thereafter, some examples have been presented. The examples compare analytical and simulated results and illustrate the benefits of a fluid compliance. Finally, two applications, an airspring (Berry, 1996) and a plastic bottle for edible oil, have been described to validate the proposed method.

2. Influence of the gas and fluid

In Fig. 1, a typical closed-filled structure has been depicted. The figure displays a closed bottle which contains both gas and fluid and is being compressed.

In the sequel, the following assumptions have been made:

- hydrostatic pressure effects of the liquid are negligible in comparison with the pressure effects of the gas;
- the gas behaves as an ideal gas;
- the temperature is constant;
- a constant amount of gas.

The virtual work corresponding to the pressure difference, can be expressed as

$$\delta W_{\mathrm{p}}^{\mathrm{ext}} = \big(p(V_{\mathrm{g}}) - p_{\mathrm{a}}\big)\delta V_{\mathrm{g}}, \tag{1}$$

where $p(V_{\mathrm{g}})$ represents the internal pressure which is a function of the gas volume, V_{g}. In case of a constant amount of ideal gas and at constant temperature the gas law simplifies to

$$pV_{\mathrm{g}} = p^0 V_{\mathrm{g}}^0 = C_{\mathrm{g}}, \tag{2}$$

where p^0, V_{g}^0 and C_{g} are the initial gas pressure, the initial gas volume and a constant, respectively (see also Fig. 1). In the present setting, it is more convenient to express the gas law in terms of the enclosed volume, V. In case the gas is governed by Eq. (2), the pressure is determined by

$$p = \frac{p^0\left(V^0 - V_{\mathrm{f}}^0\right)}{V - V_{\mathrm{f}}^0}, \tag{3}$$

where V_{f}^0 and V^0 are the initial fluid volume and the initial enclosed volume, respectively (see also Fig. 1). Introducing

$$f = \frac{V_{\mathrm{f}}^0}{V^0}, \quad v = \frac{V}{V^0}, \quad r = \frac{p}{p^0}, \tag{4}$$

where f, v, r are the initial fluid fraction, the actual volume fraction and a normalized pressure, respectively, Eq. (3) can be rewritten as

$$r = \frac{1-f}{v-f}. \tag{5}$$

As will be shown later, also the derivative of the pressure with respect to the volume will be required. This derivative can be found by differentiation of Eq. (5), giving

$$\frac{\mathrm{d}p}{\mathrm{d}V} = \frac{\mathrm{d}r}{\mathrm{d}v}\frac{p^0}{V^0} = -\frac{r}{v-f}\frac{p^0}{V^0}.$$

During a FE calculation it can occur that $v < f$. This happens when the volume change caused by a linearized step of the analysis is larger than the current gas volume leading to a new gas volume, $v-f$, which is negative. This will consequently result in a negative pressure. This has been illustrated in

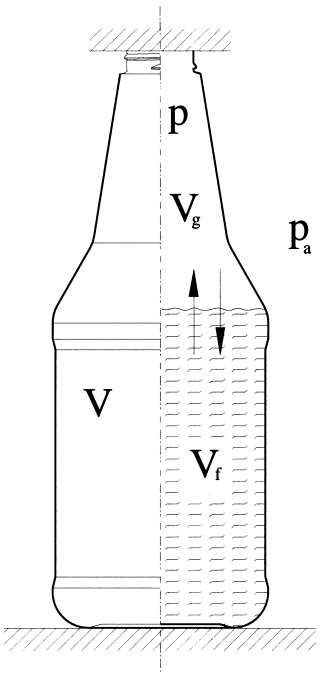

Fig. 1. Situation sketch, V, V_{g}, V_{f}, p and p_{a} are the total enclosed volume, the gas volume, the actual fluid volume, the internal pressure and the ambient pressure, respectively.

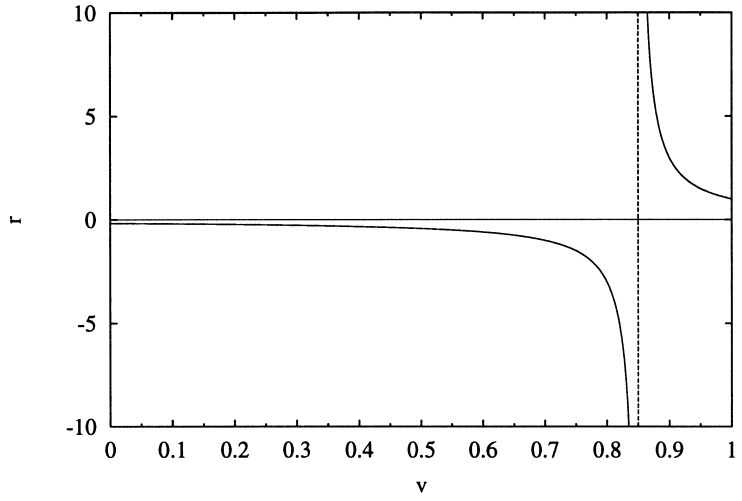

(a)

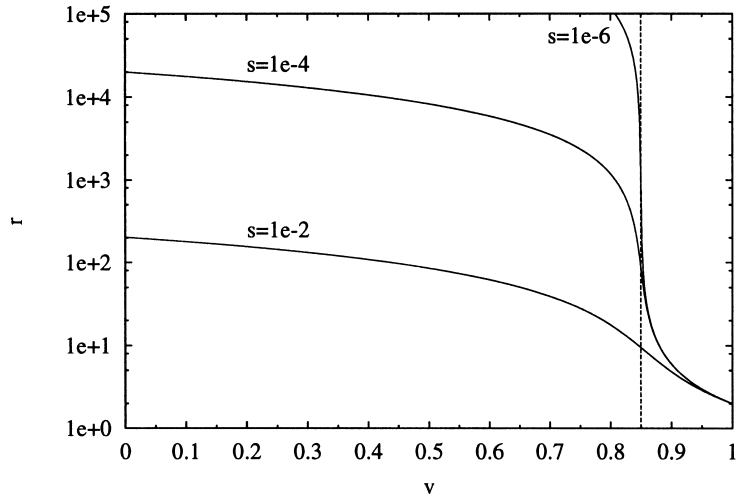

(b)

Fig. 2. The influence of fluid compressibility for a structure filled with 85% fluid. Analytical results are depicted. The horizontal and vertical axes refer to the normalized volume and the normalized pressure, respectively. (a) Due to an incremental-iterative solution procedure the gas pressure can become negative. (b) The introduction of a nearly incompressible fluid with a fluid compliance s, prevents the gas pressure from becoming negative for the full range of v. The pressure fraction r has been depicted for various values of s.

Fig. 2(a) where Eq. (5) has been plotted. Complications due to a negative pressure can be circumvented by introducing a penalty factor (Hughes, 1987, pp. 196–197) for the fluid compressibility. The penalty factor is defined as

$$c = (p - p^0)\frac{V_f^0}{V_f^0 - V_f}, \tag{6}$$

where c is the compressibility of the fluid. In case of an incompressible fluid, the compressibility c becomes infinite and consequently $V_f = V_f^0$. The total volume V is given by $V_g + V_f$ and can be expressed in terms of the internal pressure using Eqs. (2) and (6). This gives

$$V = \frac{p^0}{p} V_g^0 + \left(1 - \frac{p - p^0}{c}\right) V_f^0.$$

Similar to Eq. (4) the pressure, volume and fluid volume can be normalized. Furthermore, $f = V_f^0/V^0$ and $V^0 = V_g^0 + V_f^0$ can be combined to $(1 - f) = V_g^0/V^0$.

With the introduction of a normalized compliance for the fluid, $s = p^0/c$, the normalized pressure can be written as

$$1 - f - rv + rf - sf(r^2 - r) = 0. \tag{7}$$

Solving Eq. (7) for r is straightforward. However, only the positive solution is relevant, which reads

$$r = \frac{1}{2}\frac{f - v + sf + q}{sf}, \tag{8}$$

where

$$q = \sqrt{(f - v + sf)^2 - 4sf^2 + 4sf}.$$

Similar to Eq. (5) the derivative of the pressure with respect to volume can be evaluated, which becomes

$$\frac{dp}{dV} = -\frac{r}{q}\frac{p^0}{V^0}.$$

In Fig. 2(b), the pressure fraction, r, has been depicted for various values of s. This figure shows that s should be small such that the behavior of the structure is similar when containing an incompressible fluid. In Section 4, the effectiveness of the above approach will be illustrated on the basis of several numerical examples.

3. Finite element approach

In a general FE setting (Bathe, 1996; Zienkiewicz, 1989) we often start from the principal of virtual work which reads

$$\delta W^{\text{int}} = \delta W^{\text{ext}}, \tag{9}$$

where δW^{int} and δW^{ext} are the internal and external virtual work, respectively.

Assuming linear elastic material behavior the internal virtual work can be formally described as

$$\delta W^{\text{int}} = \delta\boldsymbol{\varepsilon}^{\mathrm{T}}\sigma = \delta\boldsymbol{\varepsilon}^{\mathrm{T}}\mathbf{S}\boldsymbol{\varepsilon}(\mathbf{u})$$

where $\varepsilon, \sigma, \mathbf{u}$ and $\mathbf{S}$ are the generalized deformations, the generalized stresses, the nodal degrees of freedom and a symmetric matrix which depends on the elastic material properties and the precise element definitions, respectively.

The corresponding rate equations become

$$\left(\mathbf{D}^{\mathrm{T}}\mathbf{S}\mathbf{D} + \mathbf{G}\right)\frac{\mathrm{d}\mathbf{u}}{\mathrm{d}\lambda} = \frac{\mathrm{d}\mathbf{f}}{\mathrm{d}\lambda}.$$

The matrix $\mathbf{G}$ represents the geometric stiffness matrix. The matrix $\mathbf{D}$ gives the relations between the deformation rates and the nodal velocities. The last term, the load vector $\mathbf{f}$, can in the present setting be described by two terms

$$\boldsymbol{f} = \lambda\mathbf{f}^{\lambda} + \mathbf{f}^{p},$$

where $\lambda\mathbf{f}^{\lambda}$ is an external load vector, independent of $\mathbf{u}$, which can be scaled with the load factor λ. The vector $\mathbf{f}^{p}$ is the external load due to the gas which, with the help of Eq. (1), can be written as

$$\mathbf{f}^{p} = \left(p\left(V_{\mathrm{g}}\right) - p_{\mathrm{a}}\right)\frac{\partial V}{\partial \mathbf{u}} \tag{10}$$

The way in which the enclosed volume of the structure is calculated, is described in Appendix A. During a FE analysis the external load will be incremented by changing the factor λ. The corresponding rate equations become

$$\left[\left(\mathbf{D}^{\mathrm{T}}\mathbf{S}\mathbf{D} + \mathbf{G}\right) - \frac{\partial \mathbf{f}^{p}}{\partial \mathbf{u}}\right]\frac{d\mathbf{u}}{d\lambda} = \mathbf{f}^{\lambda}. \tag{11}$$

With Eq. (10) it follows that

$$f^{\,p}_{i,\,j} = \frac{\mathrm{d}p\left(V_{\mathrm{g}}\right)}{\mathrm{d}V}V_{,i}V_{,j} + \left(p\left(V_{\mathrm{g}}\right) - p_{\mathrm{a}}\right)V_{,ij}, \tag{12}$$

where $\ldots_{,i}$ refers to $\frac{\partial \ldots}{\partial u_i}$.

It may be clear, that V is a function of nearly all nodal degrees of freedom. Therefore, the first term in the rhs. of Eq. (12) yields a *non-sparse* contribution to the system matrix. The contribution $f^{\,p}_{i,\,j}$ is symmetric and has previously been examined by many investigators (Hibbit, 1979; Mang, 1980; Schweizerhof and Ramm, 1984; Loganathan et al., 1979; Weingarten et al., 1965) (the reader has also referred to Appendix A). The non-sparse system matrix requires a special method to solve the set of equations using a direct method. Combining Eqs. (11) and (12) in such a way that the sparse and non-sparse components are separated leads to

$$\left[\mathbf{K} + \kappa\mathbf{a}\mathbf{a}^{\mathrm{T}}\right]\frac{\mathrm{d}\mathbf{u}}{\mathrm{d}\lambda} = \mathbf{f}^{\lambda}, \tag{13}$$

with

$$\mathbf{K} = \mathbf{D}^{\mathrm{T}}\mathbf{S}\mathbf{D} + \mathbf{G} - (p - p_{\mathrm{a}})\frac{\partial^{2} V}{\partial \mathbf{u}\partial \mathbf{u}}$$

$$\kappa = -\frac{\mathrm{d}p}{\mathrm{d}V}, \qquad \mathbf{a} = \frac{\partial V}{\partial \mathbf{u}}.$$

As can be seen from Eq. (13), $\mathbf{K}$ is still sparse, whereas the non-sparse contribution has been described by $\kappa\mathbf{a}\mathbf{a}^{\mathrm{T}}$. A technique to solve Eq. (13) has been found by trying

$$\frac{d\mathbf{u}}{d\lambda} = \mu\mathbf{a} + \mathbf{b}, \qquad \mathbf{a}\cdot\mathbf{b} = 0.$$

This results in

$$\mathbf{b} = \mathbf{K}^{-1}\mathbf{f}^{\lambda} - \mu\left(\mathbf{a} + \kappa a^2\mathbf{K}^{-1}\mathbf{a}\right)$$

with

$$\mu = \frac{\mathbf{a}^{\mathrm{T}}\mathbf{K}^{-1}\mathbf{f}^{\lambda}}{a^2\left(1 + \kappa\mathbf{a}^{\mathrm{T}}\mathbf{K}^{-1}\mathbf{a}\right)}, \qquad a^2 = \mathbf{a}^{\mathrm{T}}\mathbf{a}.$$

This way of solving is similar to the Sherman–Morrison formula (Akgün et al., 1998; Golub and van Loan, 1989; Hager, 1989) where the inverse of a modified matrix is related to the original matrix. Akgün et al. (1998) uses the Sherman–Morrison formulas for fast static reanalysis in order to find the response of a structure after modifications by using the original response of the structure. The required computional effort for this is much less than the effort required by a complete analysis. The Sherman–Morrison formulas utilize the property that the solution of a system of linear equations can be updated inexpensively when the matrix is changed by a low-rank increment (Akgün et al., 1998).

More details and a slightly modified formulation, which is also applicable when the matrix $\mathbf{K}$ is singular, are given in Appendix B. It is noted, that the problem of a non-sparse matrix could also be circumvented using a Lagrange multiplier formulation. In that case the formulation starts of from the introduction of an additional kinematic variable, being the volume of the structure. This approach will lead to governing equations which are similar to the ones described here.

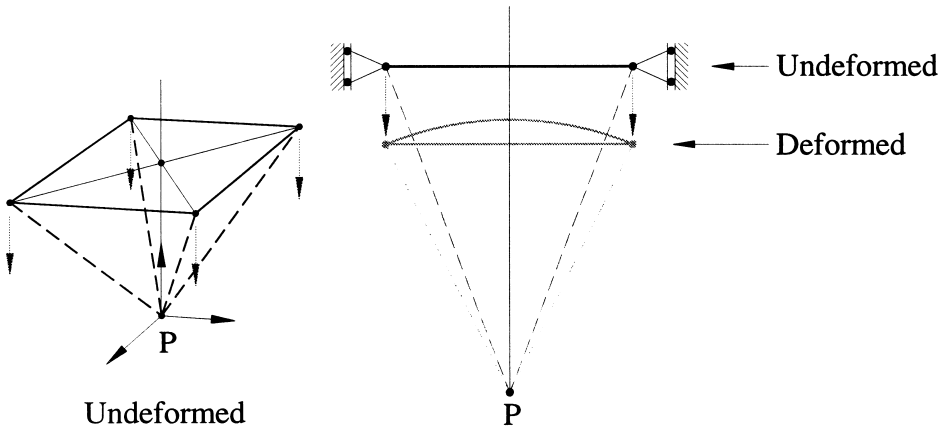

Fig. 3. Square plate that determines a pyramid shaped reference volume. The reference volume can contain a combination of fluid and gas.

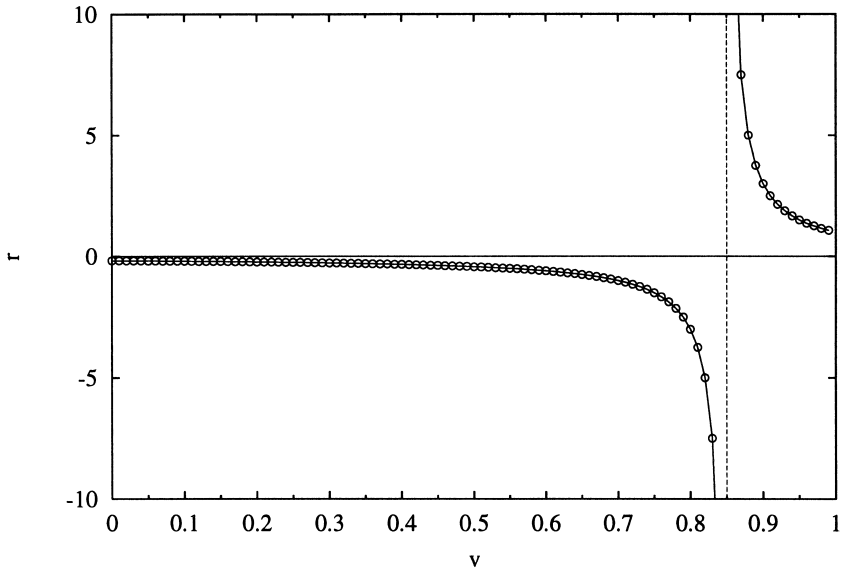

(a)

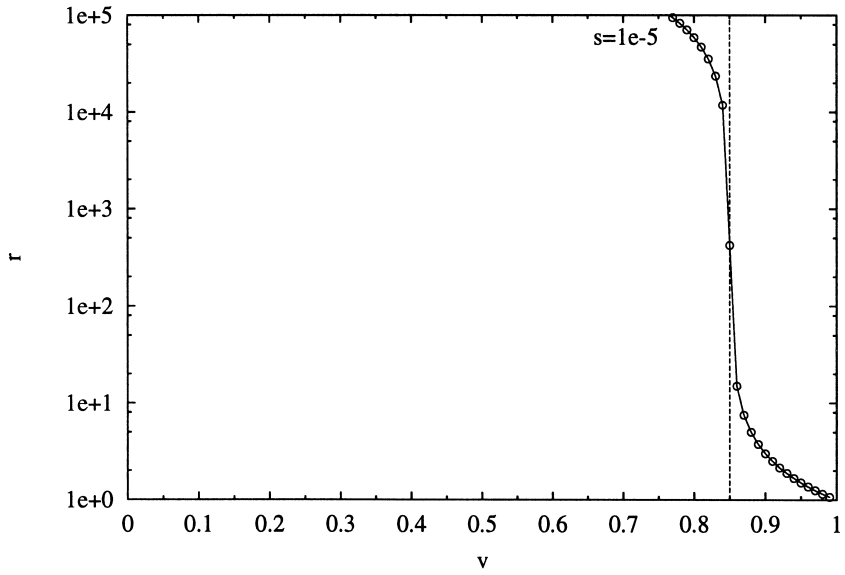

(b)

Fig. 4. Simulated compression of a rigid structure filled with 85% fluid. The horizontal axes refer to the normalized volume, whereas the vertical axes refer to the normalized pressure. (a) Structure with an incompressible fluid. (b) Structure with a nearly incompressible fluid.

4. Examples

In this section the effectiveness of the penalty method as defined by Eq. (6) will be examined by four examples, namely:

- an undeformable structure containing an incompressible fluid;
- an undeformable structure that contains a nearly incompressible fluid;
- a flexible structure containing an incompressible fluid;
- a flexible structure that contains a nearly incompressible fluid.

All four examples are based on the same problem definition. The structure that has been considered is

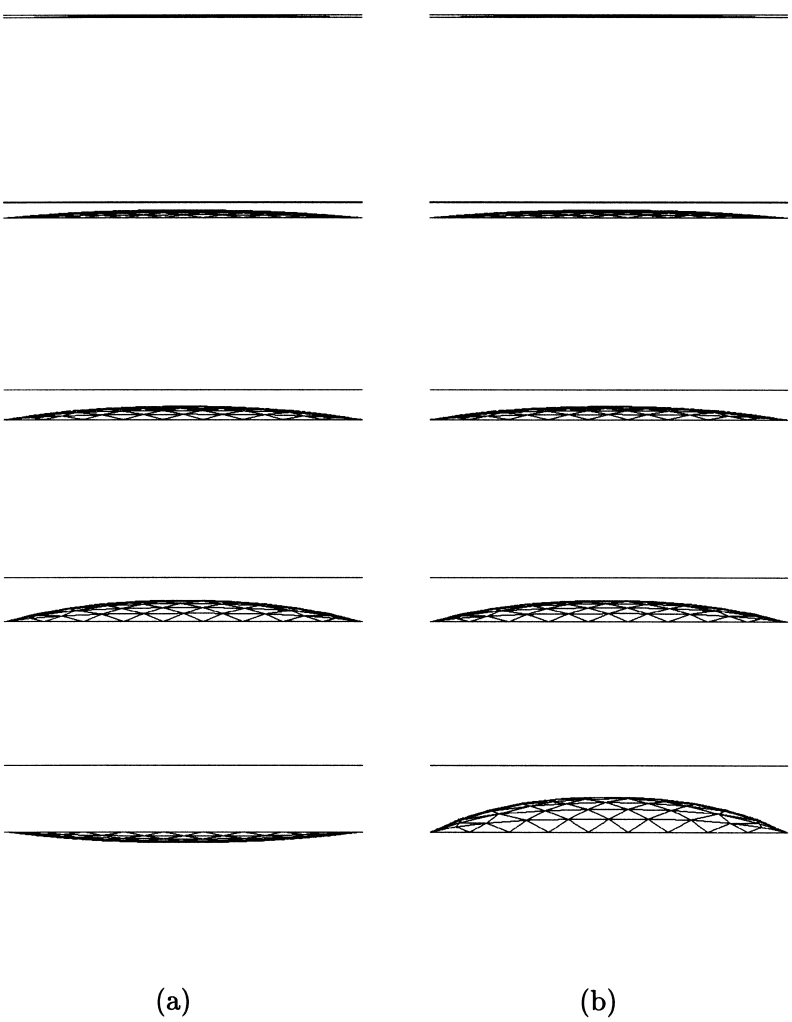

Fig. 5. Deformed configurations of a flexible structure filled with 85% fluid. Two series of subsequent configurations have been depicted. The horizontal lines depict the undeformed configuration. The applied load increases in the downward direction. (a) Deformation of the structure with an incompressible fluid. (b) Deformation of the structure with a nearly incompressible fluid.

depicted in Fig. 3, which shows a square plate that determines a pyramid shaped reference volume. The reference volume is filled with 85% fluid. A displacement in downward direction has been prescribed along all sides. The in-plane displacement components and all the rotations about the sides have been set to zero. During the downward movement of the plate the internal pressure will increase and causes deformation of the flexible plate. If during an FE analysis the volume change of the structure is larger than the remaining gas volume and the fluid is incompressible then the pressure becomes negative as discussed in Section 2. This is more prone to happen with stiff structures and can be circumvented by application of the penalty method.

The undeformable structure consists of a square plate modeled by only two triangular elements (van Keulen and Booij, 1996; van Keulen et al., 1993; Booij and van Keulen, 1994). The used element has a rotational degree of freedom about each element side and three translational degrees of freedom at each corner node. Since, the rotations about the sides of the structure have been set to zero and only two elements are used, the model will remain flat. As can be seen in Fig. 4, the pressure becomes negative in case of an incompressible fluid and remains positive in case of a nearly incompressible fluid. These results match with the analytical results as depicted in Fig. 2. Notice, that the reference volume remains a pyramid with flat faces, which is a consequence of the too coarse model, which consist of only two elements.

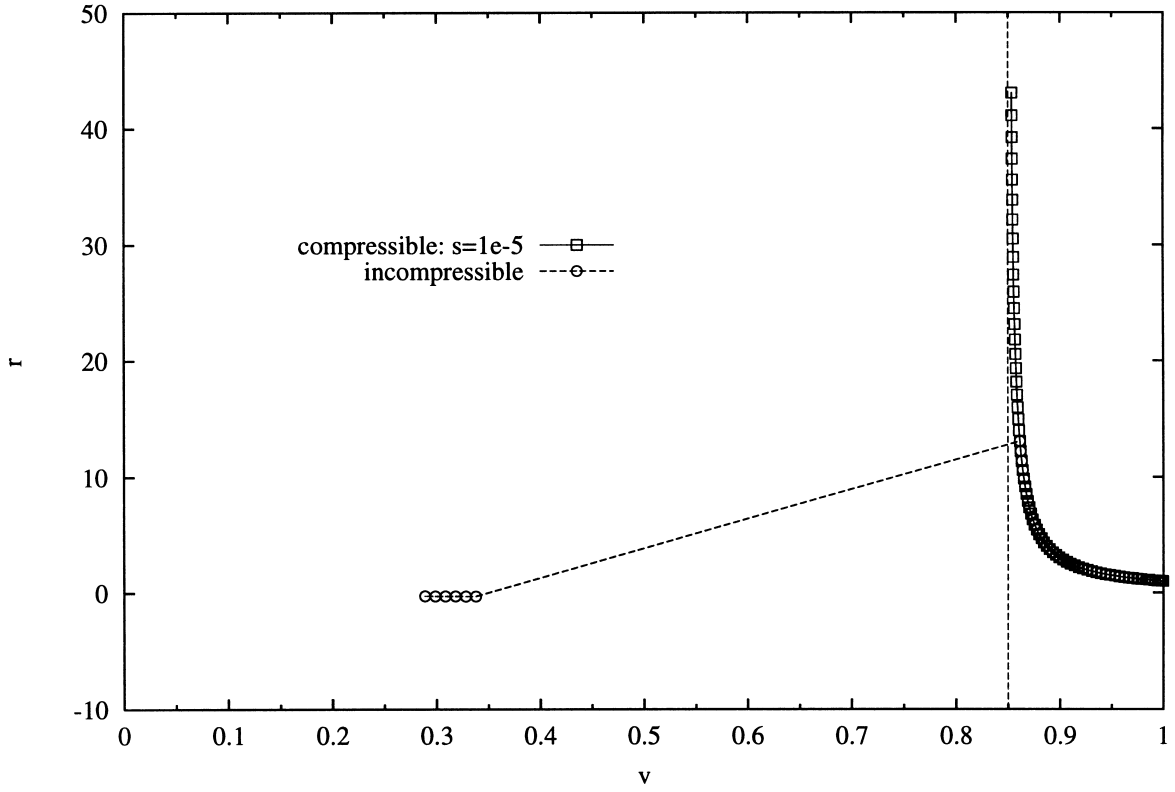

Fig. 6. Simulated compression of a flexible structure filled with 85% fluid. The horizontal axis refers to the normalized volume, whereas the vertical axis refers to the normalized pressure. Two simulations have bee depicted: with (compressible) and without penalty factor (incompressible).

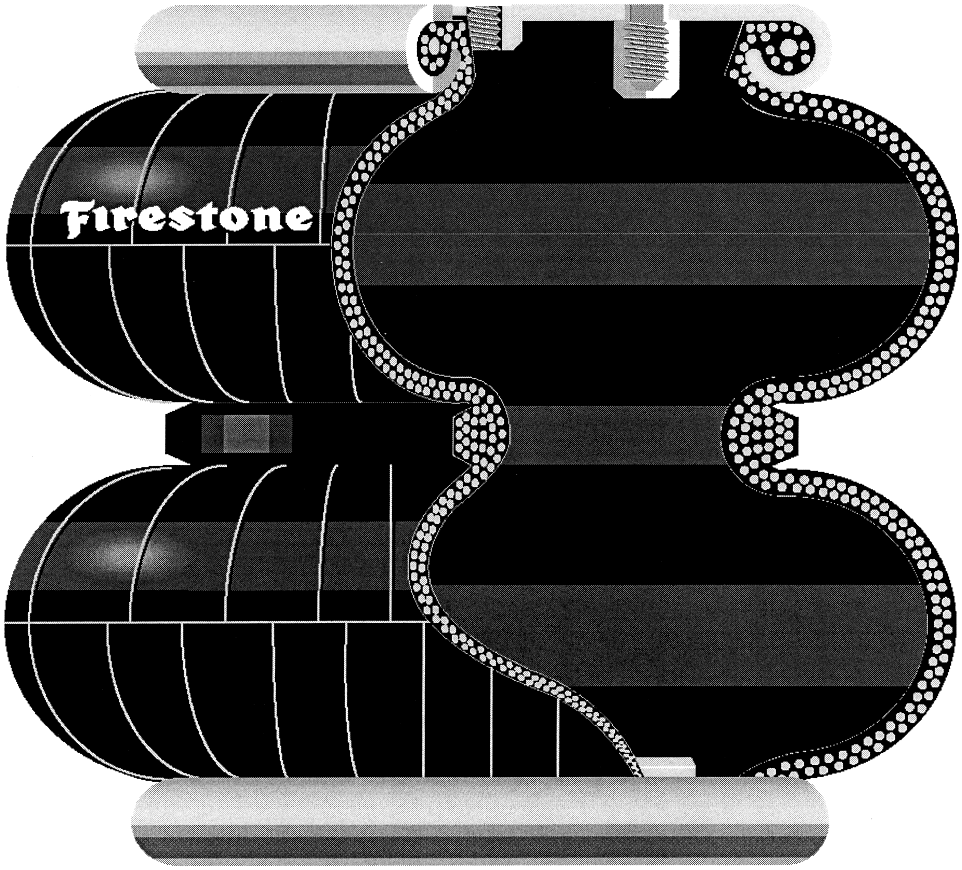

Fig. 7. The two-bellowed airspring (by courtesy of Firestone, 1997).

The flexible structure consists of a square plate modeled using a fine mesh (see Fig. 5). As can be seen in Fig. 6 the pressure becomes negative in case of an incompressible fluid and causes the curvature of the deformed configuration to reverse (see Fig. 5(a)). In case of a nearly incompressible fluid the pressure remains positive.

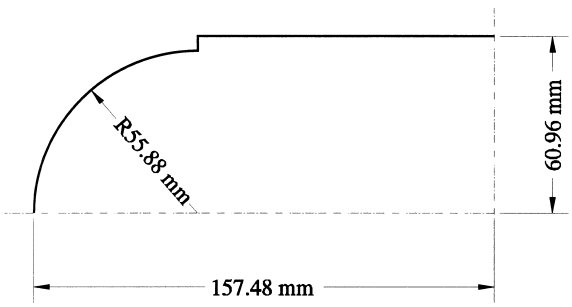

Fig. 8. Dimensions of the airspring as used in the model.

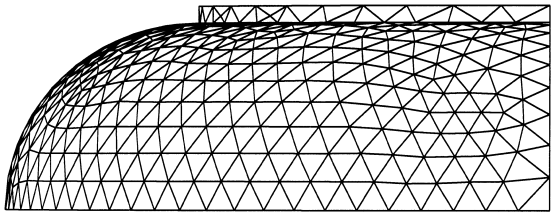

Fig. 9. Mesh of the airspring model.

5. Application

Two applications for which the pressure influence plays a significant role will be described. The first example is an airspring that has been studied by Berry (1996). The second example is a plastic bottle for edible oil.

An airspring is an air-filled reinforced rubber balloon held fixed between two rigid end plates. As the end plates are moved up and down, the internal volume expands or contracts, providing the additional pressure to support the loads. Nearly all of the load carrying capacity of the airspring is contributed by the enclosed air (Berry, 1996). The two-bellowed airspring, as used by Berry has been depicted in Fig. 7.

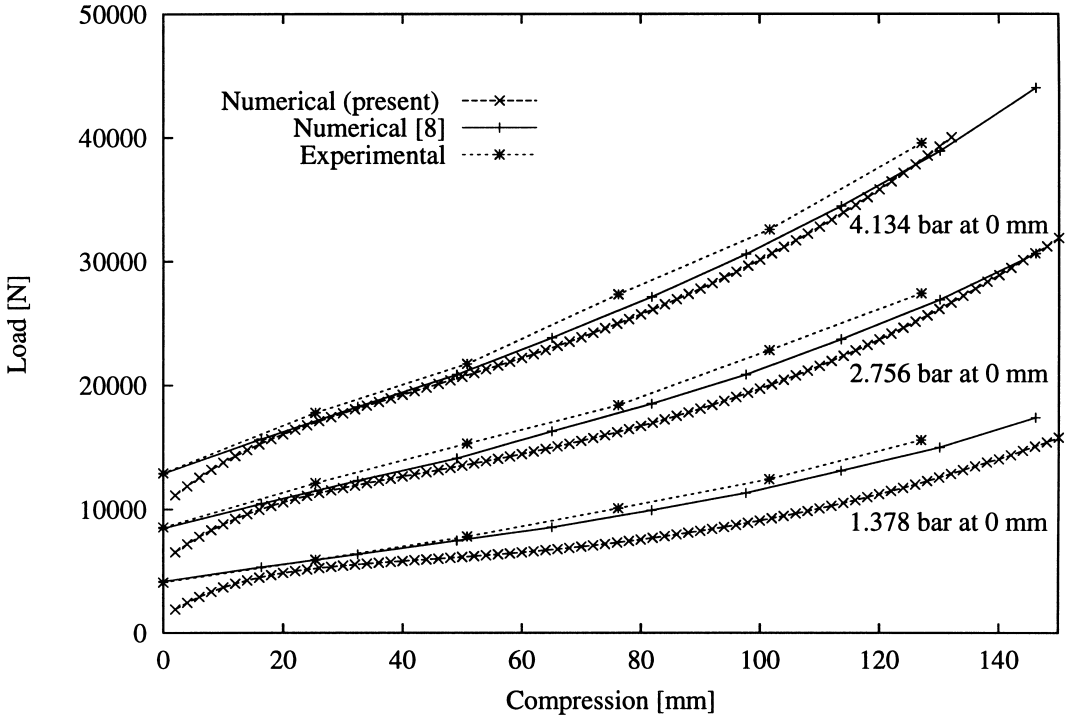

Fig. 10. Experimental and simulated results for the airspring example. The horizontal axis refers to the compression of the airspring, the vertical axis gives the required compression force. The pressures 1.378, 2.756 and 4.134 bar are initial internal pressures at 0 mm compression.

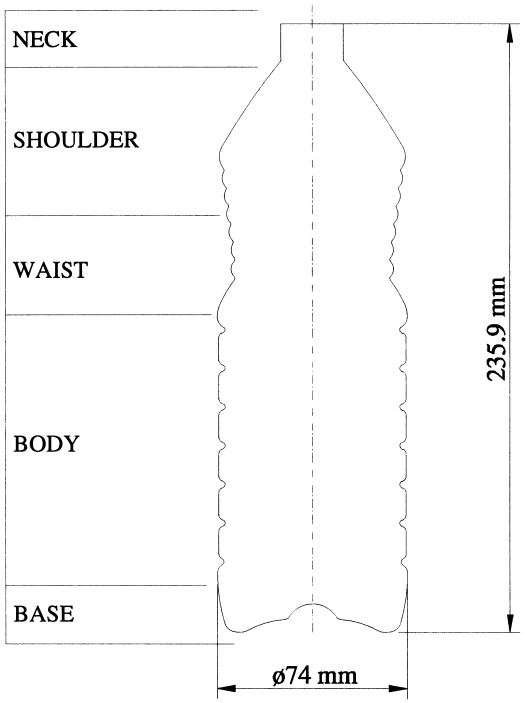

Fig. 11. Geometry of the 750 ml round oPET bottle used for packing edible oil.

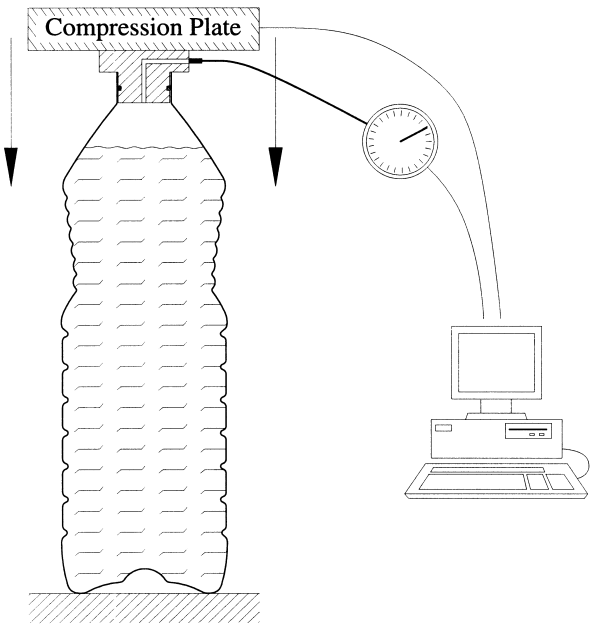

Fig. 12. Experimental setup of the pressure and top load measurements.

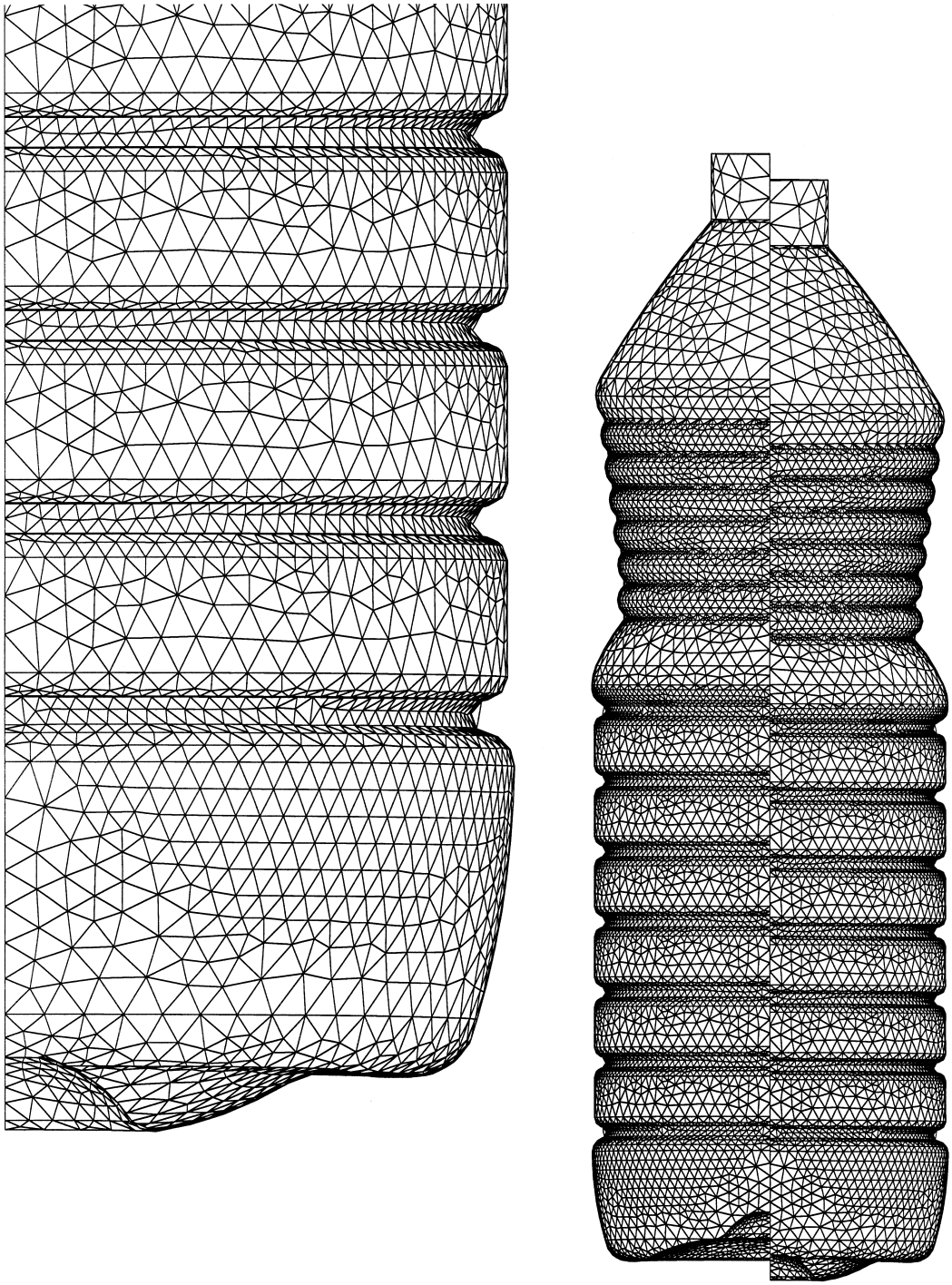

Fig. 13. Simulated deformation of a nearly full bottle under top load. This figure depicts a bottle far past its initial buckling. Since the bottle was supported on the outer diameter only (the bottle was standing on a ring), the high internal pressure caused the bottom to buckle outwards. The last is in agreement with experimental results.

Due to symmetry Berry used an axisymmetric model as depicted in Fig. 8, which also depicts the dimensions of the spring. The airspring is made out of rubber reinforced by two layers of polyester cords, which causes the spring to have a very high membrane stiffness and a very low bending stiffness. The results from Berry have been compared with results obtained by the present approach. For this a $\frac{1}{16}$ model of the airspring was modeled using triangular elements (Booij and van Keulen, 1994; van Keulen et al., 1993; van Keulen and Booij, 1996). The model had the dimensions as depicted in Fig. 8 and isotropic material properties (Young's modulus: 3000 N/mm^2, Poisson's ratio: 0.35) are used. The airspring is modeled with a thickness of 2 mm. It can be expected that for low internal pressures the load-compression curve will be different as compared to the results of Berry (1996) due to the usage of different material properties. However, at higher pressures this effect should decrease. The mesh of the model has been depicted in Fig. 9, on all sides, except the sides at the top, symmetry conditions have been applied.

On the top surface of the airspring displacements in downward direction have been prescribed. The initial internal volume has been set to 1.3257×10^7 mm^3, which is conform the actual internal volume of the airspring. Simulations have been carried out for 3 different initial pressures (1.378, 2.756 and 4.134 bar at 0 mm compression). This is conform the experiments as described by Berry (1996), where the airspring was clamped between two horizontal platen, after which the initial internal pressure was increased to the desired initial internal pressure. The results from simulations and experimental results (Berry, 1996) have been depicted in Fig. 10. This figure also shows that for small internal pressures, as

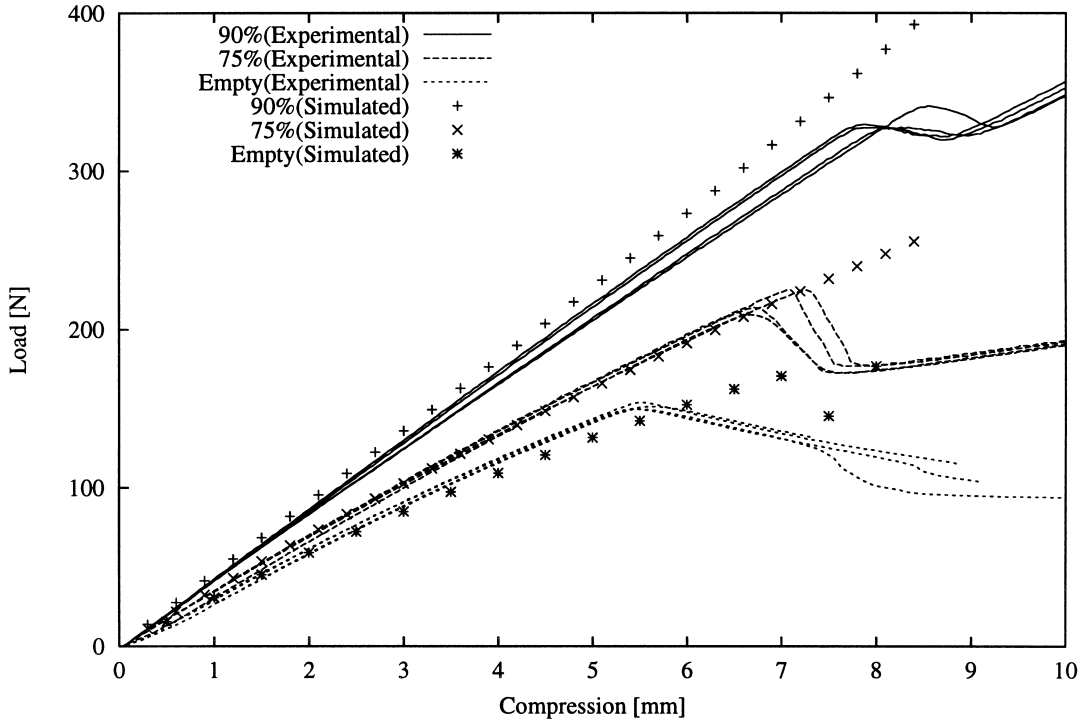

Fig. 14. Experimental and numerical results for a bottle filled with 90, 75 and 0%(empty) of fluid. The compression and the required compression load have been plotted on the horizontal and vertical axis, respectively. Note, that lines have been used for experimental results.

mentioned before, results differ due to different material properties. This explains why the results for an initial pressure of 1.378 bar differ relatively more from the calculated and experimental results of Berry (1996) than the results for higher initial pressures.

The second example describes the influence of the internal pressure for a plastic bottle for edible oil. The bottle as depicted in Fig. 11 is a 750 ml oPET (oriented PET) stretch-blown bottle for vegetable oil. During compression of the bottle, for example caused by stacking, a significant pressure increase occurs in the bottle. Several bottles, with different fill levels have been studied experimentally and afterwards simulations have been carried out for validation of the described model. In Fig. 12 the experimental set up has been depicted. During the experiments the bottle was closed with a plug. A small channel inside the plug and a narrow metal tube connected the headspace with the barometer. From several bottles the compression force, the internal (over)pressure and the vertical compression were evaluated and recorded on a computer. In all simulations triangular elements (Booij and van Keulen, 1994; van Keulen et al., 1993; van Keulen and Booij, 1996), and linear material behavior have been used. The finite element model of the bottle is depicted in Fig. 13. As can be seen in Fig. 14 the calculated and measured results match well. The fact that the buckling load of the bottle is not adequately described during the simulations can be appointed to the used material properties and the fact that initial imperfections in geometry and wall thickness distribution have not been taken into account (van Dijk, 1997; van Dijk et al., 1998). The figure clearly points out that the internal pressure significantly contributes to the strength and stiffness of the structure. The difference between experimental and calculated results at higher internal pressures for a bottle filled for 90% with fluid is caused by solubility effects which have not been taken into account. One might expect that at higher pressures and small gas–fluid ratios, the effect of gas components (in this case oxygen and nitrogen) dissolving in fluid becomes more pronounced.

In current practice the bottle is filled for 96.8% or more with fluid. In the present paper only bottles filled up to 90% have been examined, higher fill levels require inclusion of the solubility effect (van Dijk et al., 1999) which is beyond the scope of the present paper.

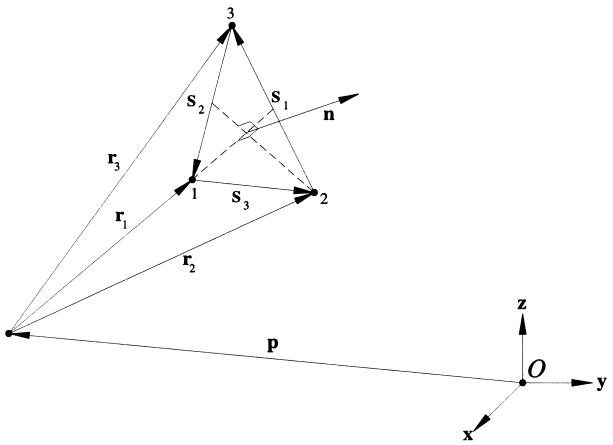

Fig. 15. Element, reference point and origin.

6. Conclusions

Many structures enclose a certain volume. Often this volume is filled with gas whereas in other structures a combination of fluid and gas is present. The gas enclosed by a structure can significantly contribute to the strength and stiffness. The methods to solve the governing equations as described in the present paper take this pressure effect into account even when the initial stiffness matrix is singular and preserve the sparse structure of the system matrix. The complication of a singular modified stiffness matrix (**K**) has been addressed in Appendix B. In most cases the approach discussed in Section 3 will be most efficient. Notice, that only in rare cases the modified system matrix will be singular. The implementation of the solution procedure which is applicable to singular initial stiffness matrices (Appendix B) is significantly more involved as compared to the formulation presented in Section 3.

Some complications can occur when during a FE analysis the volume change during a linearized step is larger than the remaining gas volume. When the fluid is incompressible this leads to negative internal pressure. Obviously, this situation is physically infeasible. The last can be circumvented by introduction of a fluid compliance. This compliance should be chosen very small in order not to affect the fluid volume in the structure.

The proposed model and its implementation has been verified by two practical examples has finally been verified by two practical examples, namely an airspring and a plastic bottle. The calculated results were in good agreement with the experimental results. As for the airspring example adequate information on material data is missing, results indicate discrepancies for low internal pressures. However, as soon as the mechanical behaviour is dominated to a significant extent by the internal pressure, numerical and experimental results are in perfect agreement. In case the amount of gas is small as compared to the fluid volume, deviations with experimental results tend to be large. This effect is due to solubility effects which play a crucial role for small gas-fluid ratios. This aspect will be the subject of a forthcoming paper.

Acknowledgements

This research was supported by Unilever Research in Vlaardingen, The Netherlands.

Appendix A

A.1. Calculation of the enclosed volume

The volume enclosed by the structure can be determined straightforwardly. In Fig. 15 a triangular element (van Keulen and Booij, 1996; van Keulen et al., 1993; Booij and van Keulen, 1994) has been depicted with a fixed reference point, **p**. The total enclosed volume of a closed structure can be determined by

$$V = \sum_{k=1}^{n} V_k, \tag{A1}$$

where k, n and V_k are the element number, the total number of elements and the contribution of a single element to the reference volume, respectively. The contribution of a single element to the reference volume is defined by the tetraedrical volume which is defined by the reference point, **p**, and the corner nodes of the element. This volume can be calculated using

$$V_k = \frac{1}{6}\mathbf{r}_1 \cdot (\mathbf{r}_2 \times \mathbf{r}_3), \tag{A2}$$

where $\mathbf{r}_1, \mathbf{r}_2$ and $\mathbf{r}_3$ are the position vectors of the corner nodes with respect to the reference point $\mathbf{p}$. These vectors span the tetraeder and are depicted in Fig. 15. In every configuration the vectors $\mathbf{r}_i$ are determined by

$$\mathbf{r}_i = \mathbf{x}_i + \hat{\mathbf{u}}_i - \mathbf{p},$$

where $\mathbf{x}_i$ and $\hat{\mathbf{u}}_i$ are the initial corner node location vectors and the nodal displacement vectors, respectively.

A.2. First-order derivatives of the volume

From Eq. (A2) the first-order variations of the volume can be determined, giving

$$\delta V_k = \frac{1}{6}\delta\mathbf{r}_1 \cdot (\mathbf{r}_2 \times \mathbf{r}_3) + \frac{1}{6}\mathbf{r}_1 \cdot (\delta\mathbf{r}_2 \times \mathbf{r}_3) + \frac{1}{6}\mathbf{r}_1 \cdot (\mathbf{r}_2 \times \delta\mathbf{r}_3).$$

After rearranging and substitution of $\delta\mathbf{r}_i = \delta\hat{\mathbf{u}}_i$, δV_k reads

$$\delta V_k = \frac{1}{6}\left[\delta\hat{\mathbf{u}}_1^{\mathrm{T}}\delta\hat{\mathbf{u}}_2^{\mathrm{T}}\delta\hat{\mathbf{u}}_3^{\mathrm{T}}\right]\begin{bmatrix}\mathbf{r}_2 \times \mathbf{r}_3 \\ \mathbf{r}_3 \times \mathbf{r}_1 \\ \mathbf{r}_1 \times \mathbf{r}_2\end{bmatrix}. \tag{A3}$$

A.3. Second-order derivatives of the volume

The second-order variations can be obtained by differentiation of the first-order variations. With Eq. (A3) the second-order variations of the volume read

$$\delta_1\delta_2 V_k = \frac{1}{6}\left[\delta_1\hat{\mathbf{u}}_1^{\mathrm{T}}\delta_1\hat{\mathbf{u}}_2^{\mathrm{T}}\delta_1\hat{\mathbf{u}}_3^{\mathrm{T}}\right]\begin{bmatrix}\delta_2(\mathbf{r}_2 \times \mathbf{r}_3) \\ \delta_2(\mathbf{r}_3 \times \mathbf{r}_1) \\ \delta_2(\mathbf{r}_1 \times \mathbf{r}_2)\end{bmatrix}.$$

This can be rewritten as

$$\delta_1\delta_2 V_k = \frac{1}{6}\left[\delta_1\hat{\mathbf{u}}_1^{\mathrm{T}}\delta_1\hat{\mathbf{u}}_2^{\mathrm{T}}\delta_1\hat{\mathbf{u}}_3^{\mathrm{T}}\right]\Gamma\begin{bmatrix}\delta_2\hat{\mathbf{u}}_1 \\ \delta_2\hat{\mathbf{u}}_2 \\ \delta_2\hat{\mathbf{u}}_3\end{bmatrix},$$

where Γ is the following matrix

$$\Gamma = \begin{bmatrix} \cdot & \cdot & \cdot & \cdot & r_3^3 & -r_3^2 & \cdot & -r_2^3 & r_2^2 \\ \cdot & \cdot & \cdot & -r_3^3 & \cdot & r_3^1 & r_2^3 & \cdot & -r_2^1 \\ \cdot & \cdot & \cdot & r_3^2 & -r_3^1 & \cdot & -r_2^2 & r_2^1 & \cdot \\ \cdot & -r_3^3 & r_3^2 & \cdot & \cdot & \cdot & \cdot & r_1^3 & -r_1^2 \\ r_3^3 & \cdot & -r_3^1 & \cdot & \cdot & \cdot & -r_1^3 & \cdot & r_1^1 \\ -r_3^2 & r_3^1 & \cdot & \cdot & \cdot & \cdot & r_1^2 & -r_1^1 & \cdot \\ \cdot & r_2^3 & -r_2^2 & \cdot & -r_1^3 & r_1^2 & \cdot & \cdot & \cdot \\ -r_2^3 & \cdot & r_2^1 & r_1^3 & \cdot & -r_1^1 & \cdot & \cdot & \cdot \\ r_2^3 & -r_2^1 & \cdot & -r_1^2 & r_1^1 & \cdot & \cdot & \cdot & \cdot \end{bmatrix}.$$

Here, r_j^i refers to the ith component $\mathbf{r}_j$. Note, that Γ is symmetric.

Appendix B

The present appendix discusses two techniques to find the solution of

$$\left[\begin{bmatrix} \mathbf{K}^{cc} & \mathbf{K}^{c0} \\ \mathbf{K}^{0c} & \mathbf{K}^{00} \end{bmatrix} + \kappa \begin{bmatrix} \mathbf{a}^c\mathbf{a}^{c^{\mathrm{T}}} & \mathbf{a}^c\mathbf{a}^{0^{\mathrm{T}}} \\ \mathbf{a}^0\mathbf{a}^{c^T} & \mathbf{a}^0\mathbf{a}^{0^{\mathrm{T}}} \end{bmatrix}\right] \begin{bmatrix} \Delta\mathbf{u}^c \\ \Delta\mathbf{u}^0 \end{bmatrix} = \begin{bmatrix} \Delta\mathbf{f}^c \\ \Delta\mathbf{f}^0 \end{bmatrix}.$$

The unknown variables are $\Delta\mathbf{u}^c$ and $\Delta\mathbf{f}^0$, whereas $\Delta\mathbf{u}^0$ and $\Delta\mathbf{f}^c$ are the known variables. Looking at the unknowns, $\Delta\mathbf{u}^c$ only and by trying

$$\Delta\mathbf{u}^c = \mu\mathbf{a}^c + \mathbf{b}^c, \qquad \mathbf{a}^{c^{\mathrm{T}}}\mathbf{b}^c = 0, \tag{B1}$$

the following augmented set of equations can be obtained

$$\begin{bmatrix} \mathbf{K}^{cc}\mathbf{K}^{cc}\mathbf{a}^c + \kappa\left(\mathbf{a}^{c^{\mathrm{T}}}\mathbf{a}^c\right)\mathbf{a}^c & \mathbf{a}^{c^{\mathrm{T}}} \\ 0 \end{bmatrix} \begin{bmatrix} \mathbf{b}^c \\ \mu \end{bmatrix} = \begin{bmatrix} \Delta\mathbf{f}^c - \left(\mathbf{K}^{c0} + \kappa\mathbf{a}^c\mathbf{a}^{0^{\mathrm{T}}}\right)\Delta\mathbf{u}^0 \\ 0 \end{bmatrix}. \tag{B2}$$

The first approach that will be described to solve Eq. (B2) will make use of the inverse of the stiffness matrix $\mathbf{K}^{cc}$, while an alternative technique does not and is therefore applicable when $\mathbf{K}^{cc}$ is singular.

B.1. Regular stiffness matrix

The first technique assumes a regular stiffness matrix $\mathbf{K}^{cc}$. From Eq. (B2) it can be determined that

$$\mathbf{b}^c = \mathbf{K}^{cc^{-1}}\left[\Delta\mathbf{f}^c - \left(\mathbf{K}^{c0} + \kappa\mathbf{a}^c\mathbf{a}^{0^{\mathrm{T}}}\right)\Delta\mathbf{u}^0\right] - \mu\mathbf{a}^c - \mu\kappa\left(\mathbf{a}^{c^{\mathrm{T}}}\mathbf{a}^c\right)\left(\mathbf{K}^{cc^{-1}}\mathbf{a}^c\right). \tag{B3}$$

Pre-multiplication by $\mathbf{a}^{c^{\mathrm{T}}}$ gives

$$\mu = \left[\frac{\mathbf{a}^{c^{\mathrm{T}}}\mathbf{K}^{cc^{-1}}\left(\Delta\mathbf{f}^c - \left(\mathbf{K}^{c0} + \kappa\mathbf{a}^c\mathbf{a}^{0^{\mathrm{T}}}\right)\Delta\mathbf{u}^0\right)}{\left(\mathbf{a}^{c^{\mathrm{T}}}\mathbf{a}^c\right)\left(1 + \kappa\mathbf{a}^{c^{\mathrm{T}}}\mathbf{K}^{cc^{-1}}\mathbf{a}^c\right)}\right], \tag{B4}$$

where use of $\mathbf{a}^{c^{\mathrm{T}}}\mathbf{b}^c = 0$ has been made. Combining Eqs. (B1)–(B3) leads to the solution of Eq. (B2)

$$\Delta\mathbf{u}^c = -\kappa\left[\frac{\mathbf{a}^{c^{\mathrm{T}}}\mathbf{K}^{cc^{-1}}\left(\Delta\mathbf{f}^c - \left(\mathbf{K}^{c0} + \kappa\mathbf{a}^c\mathbf{a}^{0^{\mathrm{T}}}\right)\Delta\mathbf{u}^0\right)}{\left(1 + \kappa\mathbf{a}^{c^{\mathrm{T}}}\mathbf{K}^{cc^{-1}}\mathbf{a}^c\right)}\right]\left(\mathbf{a}^{c^{\mathrm{T}}}\mathbf{a}^c\right)\left(\mathbf{K}^{cc^{-1}}\mathbf{a}^c\right) + \mathbf{K}^{cc^{-1}}\left[\Delta\mathbf{f}^c - \left(\mathbf{K}^{c0} + \kappa\mathbf{a}^c\mathbf{a}^{0^{\mathrm{T}}}\right)\Delta\mathbf{u}^0\right].$$

This technique requires only one additional back substitution in order to calculate $\mathbf{K}^{cc^{-1}}\mathbf{a}^c$ and proved very efficient. It is emphasized that the approach works only for a regular stiffness matrix.

B.2. Singular stiffness matrix

In case the initial stiffness matrix is singular the previous technique is not applicable and another approach must be followed to solve Eq. (B2). The alternative technique makes Eq. (B2) symmetrical by pre-multiplying it with

$$\mathbf{T} = \begin{bmatrix} \mathbf{I} & 0 \\ \mathbf{a}^{c^{\mathrm{T}}} & \kappa \mathbf{a}^{c^{\mathrm{T}}}\mathbf{a}^c \end{bmatrix},$$

where $\mathbf{I}$ is a unity matrix with the same dimensions as $\mathbf{K}^{cc}$. This results in

$$\begin{bmatrix} \mathbf{K}^{cc} & \mathbf{K}^{cc}\mathbf{a}^c + \kappa\left(\mathbf{a}^{c^{\mathrm{T}}}\mathbf{a}^c\right)\mathbf{a}^c \\ \left\{\mathbf{K}^{cc}\mathbf{a}^c + \kappa\left(\mathbf{a}^{c^{\mathrm{T}}}\mathbf{a}^c\right)\mathbf{a}^c\right\}^{\mathrm{T}} & \mathbf{a}^{c^{\mathrm{T}}}K^{cc}\mathbf{a}^c + \kappa\left(\mathbf{a}^{c^{\mathrm{T}}}\mathbf{a}^c\right)^2 \end{bmatrix} \begin{bmatrix} \mathbf{b}^c \\ \mu \end{bmatrix} = \begin{bmatrix} \Delta\mathbf{f}^c - \left(\mathbf{K}^{c0} + \kappa\mathbf{a}^c\mathbf{a}^{0^{\mathrm{T}}}\right)\mathbf{u}^0 \\ \mathbf{a}^{c^{\mathrm{T}}}\left(\Delta\mathbf{f}^c - \left(\mathbf{K}^{c0} + \kappa\mathbf{a}^c\mathbf{a}^{0^{\mathrm{T}}}\right)\mathbf{u}^0\right) \end{bmatrix}. \tag{B5}$$

As can be seen from Eq. (B5), the matrix on the lhs. is symmetric. In spite of the fact that the stiffness matrix $\mathbf{K}^{cc}$ can be singular, the modified matrix can be regular. The obtained augmented set of Eq. (B5) can be solved with a direct solver. A more careful inspection of Eq. (B5) reveals that only an additional row or column has to be stored

References

ABAQUS Theory Manual Version 5.5, 1995. Hibbit, Karlsson and Sorensen, 1080 Main Street, Pawtucket, USA.

Akgün, M.A., Garcelon, J.H., Haftka, R.T., 1998. Fast exact linear and nonlinear structural reanalysis and the Sherman–Morrison–Woodburry formulas. Int. J. Num. Methods in Eng., submitted.

Bathe, K.J., 1996. Finite Element Procedures. Prentice-Hall, Englewood Cliffs, NJ.

Berry, D.T., 1996. Formulation and experimental verification of a pneumatic element. Int. J. Num. Meth. Eng 39, 1097–1114.

Booij, J., van Keulen, F., 1994. Consistent formulation of a triangular finite rotation shell element. In: Kusters, G.M.A., Hendriks, M.A.N. (Eds.), Proceedings of the First International DIANA Conference on Computational Mechanics, DIANA Computational Mechanics '94, pp. 235–244.

Bucklin, R.A., Ross, I.J., White, G.M., 1985. The influence of grain pressure on the buckling load of thin walled bins. Transactions of the ASEA 28, 2011–2020.

Esslinger, M., Geier, B., 1976. Calculated postbuckling loads as lower limits for the buckling loads of thin-walled circular cylinders. Buckling of Structures, 274–290.

Firestone Industrial Products Company, 1997. Firestone Airstroke Actuators and Airmount Isolators. Engineering Manual and Design Guide (MEMDG 997), Carmel, IN, USA.

Fung, Y.C., Sechler, E.E., 1957. Buckling of thin-walled circular cylinders under axial compression and internal pressure. Journal of Aeronautical Sciences 24, 351–356.

Golub, G.H., van Loan, C.F., 1989. Matrix Computations. John Hopkins University Press, Baltimore.

Goree, W.S., Nash, N.A., 1962. Elastic stability of circular shells stabilized by a soft elastic core. Proceedings of the Society for Experimental Stress Analysis 19, 142–149.

Hager, W.W., 1989. Updating the inverse of a matrix. SIAM review 31, 221–239.

Harris, L.A., et al., 1957. The stability of thin-walled unstiffened circular cylinders under axial compression including the effects of internal pressure. Journal of Aeronautical Sciences 24, 587–596.

Hibbit, H.D., 1979. Some follower forces and load stiffness. Int. J. Numer. Methods Eng 14, 937–941.

Hughes, T.J.R., 1987. The Finite Element Method. Prentice-Hall, Englewood Cliffs, NJ.

Loganathan, K., Chang, S.C., Gallagher, R.H., Abel, J.F., 1979. Finite element representation and pressure stiffness in shell stability analysis. Int. J. Num. Methods Eng 14, 1413–1429.

Mang, H.A., 1980. Symmetricability of pressure stiffness matrices for shell with loaded free edges. Int. J. Num. Methods Eng 15, 981–990.

Schweizerhof, K., Ramm, E., 1984. Displacement dependent pressure loads in nonlinear finite element analysis. Computers and Structures 18, 1099–1114.

Seide, P., 1962. The stability under axial compression and lateral pressure of circular-cylindrical shells with a soft elastic core. Journal of the Aerospace Sciences 29, 851–862.

van Dijk, R., 1997. FEA as a design tool. Packaging Today Europe 1 (2), 40–44.

van Dijk, R., Sterk, J.C., van Keulen, F., Sgorbani, D., 1998. Lateral deformation of plastic bottles; experiments, simulations and prevention. Packaging Technology and Science 11, 91–117.

van Dijk, R., van Keulen, F., Sterk, J.C., 1999. The influence of solubility effects on the pressure increase during deformation of closed thin-walled structures. Thin-Walled Structures 35, 25–40.

van Keulen, F., Booij, J., 1996. Refined consistent formulation of a curved triangular finite rotation shell element. Int. J. Num. Meth. Eng 39, 2803–2830.

van Keulen, F., Bout, A., Ernst, L.J., 1993. Nonlinear thin shell analysis using a curved triangular element. Comp. Meth. Appl. Mech. Engng 103, 315–343.

Weingarten, V.I., Morgan, E.J., Seide, P., 1965. Elastic stability of thin-walled cylindrical and conical shells under combined internal pressure and axial compression. AIAA Journal 3, 1118–1125.

Zienkiewicz, O.C., 1989. The Finite Element Method in Engineering Science. McGraw-Hill, London.